REPORT DOCUMENTATION PAGE		Form Approved OMB NO. 0704-0188

The public reporting burden for this collection of information is estimated to average 1 hour per response, including the time for reviewing instructions, searching existing data sources, gathering and maintaining the data needed, and completing and reviewing the collection of information. Send comments regarding this burden estimate or any other aspect of this collection of information, including suggesstions for reducing this burden, to Washington Headquarters Services, Directorate for Information Operations and Reports, 1215 Jefferson Davis Highway, Suite 1204, Arlington VA, 22202-4302. Respondents should be aware that notwithstanding any other provision of law, no person shall be subject to any oenalty for failing to comply with a collection of information if it does not display a currently valid OMB control number.
PLEASE DO NOT RETURN YOUR FORM TO THE ABOVE ADDRESS.

1. REPORT DATE (DD-MM-YYYY) 09-11-2018	2. REPORT TYPE Final Report	3. DATES COVERED (From - To) 1-Aug-2014 - 31-Oct-2015
4. TITLE AND SUBTITLE Final Report: Broadband Optical Characterization of Semiconductors and Metal:Semiconductor Nanocomposites		5a. CONTRACT NUMBER W911NF-14-1-0418
		5b. GRANT NUMBER
		5c. PROGRAM ELEMENT NUMBER 611103
6. AUTHORS		5d. PROJECT NUMBER
		5e. TASK NUMBER
		5f. WORK UNIT NUMBER
7. PERFORMING ORGANIZATION NAMES AND ADDRESSES University of Texas at Austin 101 East 27th Street Suite 5.300 Austin, TX 78712 -1532		8. PERFORMING ORGANIZATION REPORT NUMBER
9. SPONSORING/MONITORING AGENCY NAME(S) AND ADDRESS (ES) U.S. Army Research Office P.O. Box 12211 Research Triangle Park, NC 27709-2211		10. SPONSOR/MONITOR'S ACRONYM(S) ARO
		11. SPONSOR/MONITOR'S REPORT NUMBER(S) 65034-EL-RIP.1

12. DISTRIBUTION AVAILIBILITY STATEMENT
Approved for public release; distribution is unlimited.

13. SUPPLEMENTARY NOTES
The views, opinions and/or findings contained in this report are those of the author(s) and should not contrued as an official Department of the Army position, policy or decision, unless so designated by other documentation.

14. ABSTRACT

15. SUBJECT TERMS

16. SECURITY CLASSIFICATION OF:			17. LIMITATION OF ABSTRACT	15. NUMBER OF PAGES	19a. NAME OF RESPONSIBLE PERSON Seth Bank
a. REPORT UU	b. ABSTRACT UU	c. THIS PAGE UU	UU		19b. TELEPHONE NUMBER 512-471-9669

Agency Code:

Proposal Number: 65034ELRIP   **Agreement Number: W911NF-14-1-0418**
INVESTIGATOR(S):

Name: PhD Seth R. Bank
Email: sbank@ece.utexas.edu
Phone Number: 5124719669
Principal: Y

Organization: **University of Texas at Austin**
Address: 101 East 27th Street, Austin, TX 787121532
Country: USA
DUNS Number: 170230239   EIN: 746000203
Report Date: 31-Jan-2016   Date Received: 09-Nov-2018
Final Report for Period Beginning 01-Aug-2014 and Ending 31-Oct-2015
Title: Broadband Optical Characterization of Semiconductors and Metal:Semiconductor Nanocomposites
Begin Performance Period: 01-Aug-2014   **End Performance Period:** 31-Oct-2015
Report Term: 0-Other
Submitted By: PhD Seth Bank   Email: sbank@ece.utexas.edu
                                                Phone: (512) 471-9669
Distribution Statement: 1-Approved for public release; distribution is unlimited.

STEM Degrees: 2   **STEM Participants:** 4

Major Goals: This instrumentation enhanced our characterization capabilities over the mid-infrared, far-infrared, THz, and sub-THz regions of the electromagnetic spectrum. Specifically, we received a Fourier transform infrared (FTIR) spectrometer/IR-microscope and associated accessories to probe the optical properties of the nanostructured materials we prepare by molecular beam epitaxy and other synthesis techniques. The requested instrumentation has enabled us to (1) optically study structures emitting/absorbing >5 microns where our grating spectrometer systems become insensitive and (2) readily characterize patterned structures electrically and optically, greatly enhancing our device characterization capabilities. For example, these capabilities have enabled us to measure the absorption properties of emergent photodetector materials, such as AlInAsSb digital alloys grown on GaSb. The instrumentation has also enabled us to directly measure the plasmonic response of doped semiconductors and semimetallic rare earth monopnictides, as well as the optical resonances associated with buried dielectric structures. This has greatly enabled our work in the burgeoning fields of epitaxial plasmonics and high-contrast photonics, which could enable the integration of plasmonic functionality into the heart of photonic devices.

This tool has established manifold new research capabilities and has already been used by roughly a dozen researchers at UT-Austin, as well as several others from other leading research universities. These critical new capabilities (lifespan 15-20 years) have dramatically enhanced the PI's current, upcoming, and long-term research efforts sponsored by DoD, while providing hands-on experience characterizing new state-of-the-art materials/devices to a number of future scientists and engineers. Moreover, the advances in nanostructured materials that this instrumentation has enabled have manifold application to future strategic DoD capabilities in (multi-modal) sensing, 3-D LIDAR, laser-based countermeasures, free-space communications, security screening, IED detection, and chemical/gas sensing.

Accomplishments: The DURIP Awards were announced at the end of May 2014; after final configuration was determined and the purchase order was placed, the lab space was renovated while the instrument was being built and shipped. The instrumentation was delivered to and installed at UT by Bruker engineers in December 2014. Bruker scientists also came for two days in March 2015 to give a seminar and train students across UT, as well as run research samples to highlight the capabilities of the instrumentation. This presentation was open to the public and was attended by >50 scientists and engineers from the greater Austin area. This tool has established manifold new research capabilities and has already been used by roughly a dozen researchers at UT-Austin, as well as several others from other leading research universities.

Training Opportunities: These critical new capabilities (lifespan 15-20 years) have dramatically enhanced the PI's current, upcoming, and long-term research efforts sponsored by DoD, providing hands-on experience characterizing new state-of-the-art materials/devices to a number of future scientists and engineers. This tool has established manifold new research capabilities and has already been used by roughly a dozen researchers at UT-Austin, as well as several others from other leading research universities.

Results Dissemination: Nothing to Report

Honors and Awards: Nothing to Report

Protocol Activity Status:

Technology Transfer: This instrumentation has not directly led to tech transfer, but has enabled much of our research progress that has led to significant tech transfer opportunities. For example, our avalanche photodiode work has generated significant interest at Night Vision Labs (which we have visited), AFRL, and Lockheed Martin. We have filed multiple patents in this area and are in discussion to license the patents.

 PARTICIPANTS:

 Participant Type: PD/PI
 Participant: Seth Robert Bank
 Person Months Worked: 1.00   **Funding Support:**
 Project Contribution:
 International Collaboration:
 International Travel:
 National Academy Member: N
 Other Collaborators:

Broadband Optical Characterization of Semiconductors and Metal:Semiconductor Nanocomposites

Abstract

This instrumentation enhanced our characterization capabilities over the mid-infrared, far-infrared, THz, and sub-THz regions of the electromagnetic spectrum. Specifically, we received a Fourier transform infrared (FTIR) spectrometer/IR-microscope and associated accessories to probe the optical properties of the nanostructured materials we prepare by molecular beam epitaxy and other synthesis techniques. The requested instrumentation has enabled us to (1) optically study structures emitting/absorbing >5 μm where our grating spectrometer systems become insensitive and (2) readily characterize patterned structures electrically and optically, greatly enhancing our device characterization capabilities. For example, these capabilities have enabled us to measure the absorption properties of emergent photodetector materials, such as AlInAsSb digital alloys grown on GaSb. The instrumentation has also enabled us to directly measure the plasmonic response of doped semiconductors and semimetallic rare earth monopnictides, as well as the optical resonances associated with buried dielectric structures. This has greatly enabled our work in the burgeoning fields of epitaxial plasmonics and high-contrast photonics, which could enable the integration of plasmonic functionality into the heart of photonic devices.

This tool has established manifold new research capabilities and has already been used by roughly a dozen researchers at UT-Austin, as well as several others from other leading research universities. These critical new capabilities (lifespan 15-20 years) have dramatically enhanced the PI's current, upcoming, and long-term research efforts sponsored by DoD, while providing hands-on experience characterizing new state-of-the-art materials/devices to a number of future scientists and engineers. Moreover, the advances in nanostructured materials that this instrumentation has enabled have manifold application to future strategic DoD capabilities in (multi-modal) sensing, 3-D LIDAR, laser-based countermeasures, free-space communications, security screening, IED detection, and chemical/gas sensing.

1. Request for Instrumentation

The PI is involved in a number of current research efforts sponsored by DoD, with application to strategic capabilities in multi-modal sensing, 3-D LIDAR, laser-based countermeasures, free-space communications, high-speed transistors, security screening, IED detection, chemical/gas sensing, energy harvesting, etc. This work is enabled by the nanoscale design and synthesis of novel materials, including metal:semiconductor nanocomposites (metallic nanostructures embedded in a semiconductor matrix) and semiconductor nanostructures, using the molecular beam epitaxy (MBE) crystal growth technique.

With this DURIP instrumentation, we enhanced our capabilities for characterizing materials and devices. In particular, the specific instrumentation is a high-resolution, broadband, Fourier transform infrared (FTIR) spectrometer with infrared microscope, as well as an optical table to serve as a platform for the instrumentation and associated experimental setups. As illustrated in the following sections, this instrumentation has greatly enhance our spectroscopy and device characterization capabilities by providing: (1) high-resolution, broadband, spectroscopy capabilities to augment our mid-infrared and THz materials work, (2) local probing of patterned structures to greatly enhance/improve materials and device characterization capabilities.

The instrumentation acquired though this DURIP award represents a strategic DoD investment opportunity to (1) enable future systems based upon new nanostructure-based device technologies and (2) educate graduate and undergraduate students in the strategically important sciences of nanostructured materials, optics, electronics, and optoelectronics.

## 2. Overview of Instrumentation and Installation

The instrumentation, shown in **Figure 1a**, has greatly enhanced the PI's current and long-term research. Specifically, to fully and expeditiously investigate the growth of novel nanostructures and emergent photonic materials, as well as demonstrate new device functionality from these materials, we require improved material/device characterization capabilities: (1) broadband spectroscopy and (2) spatially-resolved optical access.

These two measurement capabilities required two systems (**Figure 1a**) that are coupled together: (1) a high-resolution FTIR (spectral range given in **TABLE I**) and (2) an infrared microscope, as well as an optical table. These two systems have been integrated together by Bruker; additionally,

TABLE I. FTIR SPECTRAL RANGE.

Quantity	Lower Bound	Upper Bound
Wavenumber	10 cm^{-1}	15,500 cm^{-1}
Frequency	0.3 THz	465 THz
Wavelength	1,000 μm	645 nm

Bruker offers unique performance capabilities, relative to other manufacturers.[1] As discussed in the next section, the acquired instrumentation has established manifold new research avenues in manipulating and controlling the electrical and optical properties of new semiconductor alloys, semimetallic alloys, and metal:semiconductor nanocomposites, enabling novel device architectures in key DoD areas of interest including sensors and sources in the mid-IR, long-wave IR, and THz.

---

[1] *e.g.* The Bruker FTIR is protected by US 5309217; DE 4212143; US 7034944; US 5923422; DE 19704598.
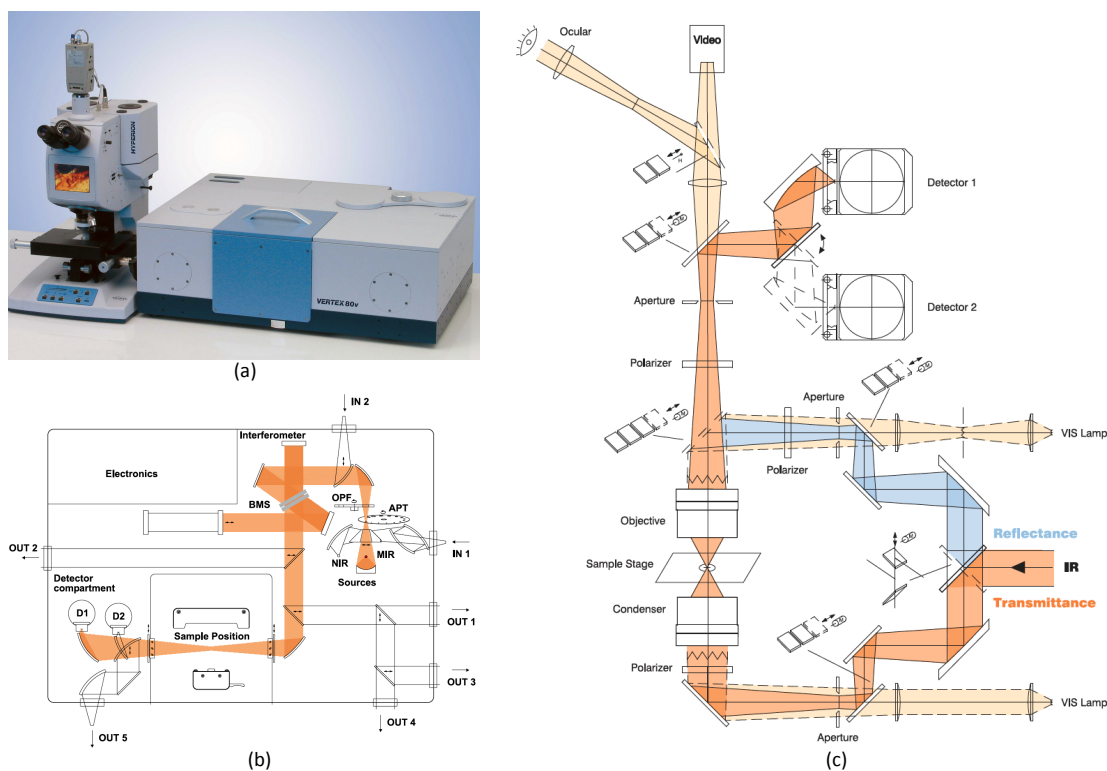
Figure 1. (a) Photograph of the interconnected Bruker v80 FTIR (right) and Hyperion IR microscope (left). Optical system of the (b) FTIR and (c) microscope. Note the extended beam path within the FTIR; in conjunction with an evacuated housing, this patented design enables extremely broadband optical response and high spectral resolution.

The DURIP Awards were announced at the end of May 2014; after final configuration was determined and the purchase order was placed, the lab space was renovated while the instrument was being built and shipped. The instrumentation was delivered to and installed at UT by Bruker engineers in December 2014, as shown in the **Figure 2**. Bruker scientists also came for two days in March 2015 to give a seminar and train students across UT, as well as run research samples to highlight the capabilities of the instrumentation. This presentation was open to the public and was attended by >50 scientists and engineers from the greater Austin area.
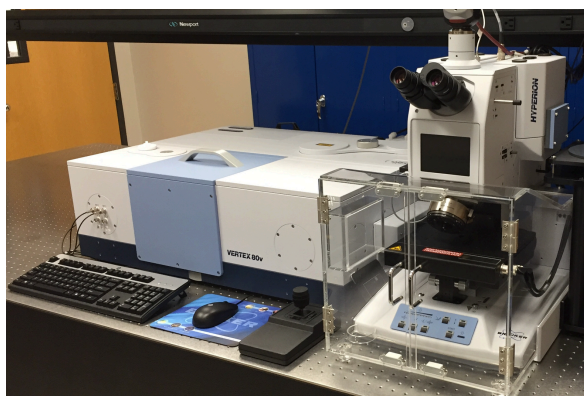
Figure 2. Photograph of the installed FTIR and IR microscope installed in the PI's lab at UT-Austin.

3

3. Examples of Research Benefitting from the Requested Instrumentation

Here, we present a few salient examples of how we have employed this instrumentation to our research to illustrate its broad applicability, for both our internal and collaborative research.

3.1. Emerging Photonic Materials

3.1.1. Doped-Semiconductor Plasmonics

There is a great need to develop nanophotonic components in the mid infrared, ~3-5 μm, for a number of applications in gas sensing, 3-D laser radar, and free-space/integrated data links at the various atmospheric transmission windows, in particular those between ~3-4 μm. Plasmonics offer the prospect of significant device scaling to reduce SWaP and increase integration density for systems, as well as for enhancing device performance and potentially realizing fundamentally new functionality.

The plasma frequency, ω_p, is essentially the highest optical frequency that a material will respond to like a metal (i.e. with a free electron plasma). To first order, ω_p is given by:

$$\omega_p \approx \sqrt{\frac{Ne^2}{m^* \varepsilon_0 n_{0,InAs}^2}}$$

where N is the active electron concentration, e is the fundamental charge, m^* is the electron effective mass, ε_0 is the permittivity of free space, and $n_{0,InAs}$ is the refractive index. Increasing the plasma frequency is straightforward to accomplish with increasing (active) doping, N.

Glazov and co-workers studied several alternative n-type dopants (sulfur, selenium, and tellurium) for InAs using direct fusion in a sealed ampoule, in concert with annealing and quenching steps [1]. Significantly higher electron concentrations were achieved with sulfur, with close to unity dopant activation $>7\times10^{20}$ cm^{-3}, close to what is required to build devices operating at 5 μm. This is a very promising avenue to pursue, particularly if higher doping concentrations could be achieved with modern kinetically-limited synthesis techniques. Through an ARO STIR Award, we sought to compare sulfur-doped InAs to our best silicon-doped InAs to evaluate whether it would be an attractive alternative to accessing shorter wavelengths with doped-semiconductor plasmonics.

Each experiment began with the MBE growth of a 200 nm layer of undoped InAs on 3-inch diameter semi-insulating GaAs wafers. Wafers were then ion-implanted with varying sulfur doses at peak concentration depths of 50 nm, providing ~100 nm of sulfur-doped InAs. This was thin enough to remain achievable by singly-ionized ion implantation, yet thick enough for accurate determination of the active carrier concentration and plasma wavelength by Hall effect and reflectivity measurements.

Optical reflectivity was performed with the FTIR spectrometer; representative results are plotted in **Figure 3**, along with a high-quality MBE-grown silicon-doped InAs sample for reference. Due to the thinner layers, which were limited by the constraints of ion implantation, the InAs:S samples did not exhibit as well-defined a Drude edge in reflectivity as the thicker InAs:Si samples. Surprisingly, the

plasma frequencies were unexpectedly low in the sulfur-doped samples, inconsistent with the calculations using the measured sheet concentrations and mobilities. We determined that the issue was sulfur diffusion, which was evident in complementary secondary ion mass spectrometry (SIMS) measurements.
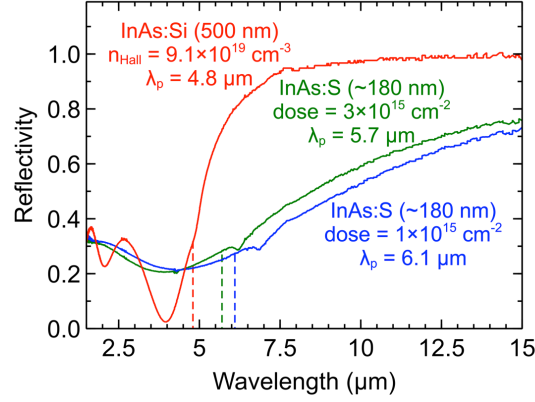

Figure 3. Optical reflectivity of InAs:S samples with implantation doses of 1×10^{15} and 3.16×10^{15} cm^{-2} sulfur atoms, compared with a reference InAs:Si. As expected, the implanted structures exhibited a more gradual Drude edge, which was attributed to the thinner doped regions; however, the measured plasma frequencies were significantly lower than expected from the Hall Effect data.


(a)   (b)   (c)
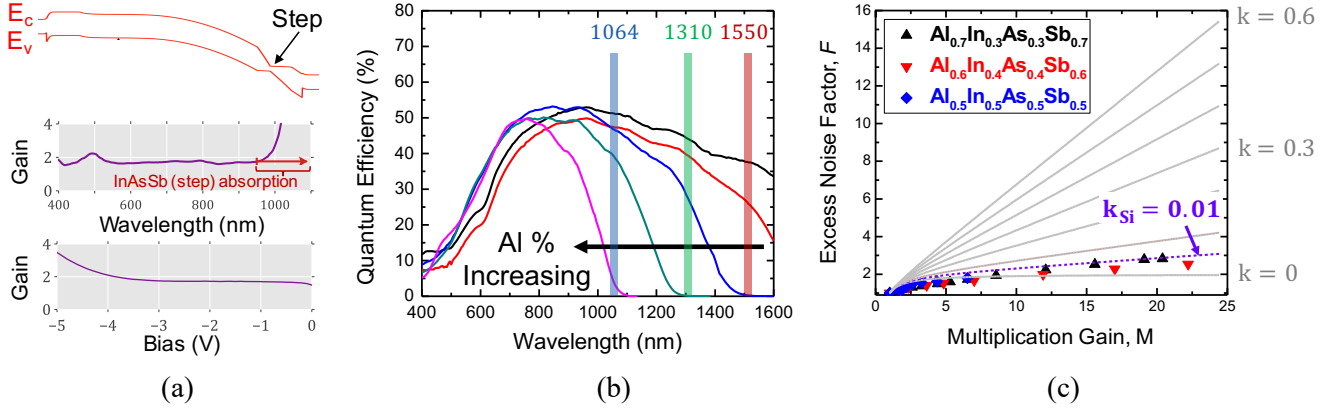
Figure 4. (a) Single step staircase APD result showing a gain of ~2x over a wide range of test conditions, consistent with theory. AlInAsSb homojunction pin detectors (b) showing tunable cutoff wavelength with composition and (c) low excess noise, comparable to that of silicon, when operated as a conventional APD.

3.1.2. Digital Alloys for Avalanche Photodiodes (APD)

Through ARO and DARPA support, we have developed the growth of AlInAsSb digital alloys, lattice-matched to GaSb substrates. In collaboration with Prof. Joe Campbell at the University of Virginia, as illustrated in **Figure 4**, these alloys uniformly exhibit low excess noise and when used as the multiplier in avalanche photodiodes (APD) and offer seamless band engineering capabilities needed for advanced detector structures like the staircase APD. The FTIR was used to study the absorption spectra by measuring the transmission and reflection signal from our digital alloy materials. **Figure 5** shows an example reflectance spectrum used to calculate the absorption coefficients of the bulk digital alloy samples. These measurements were performed by an NSF summer REU student.
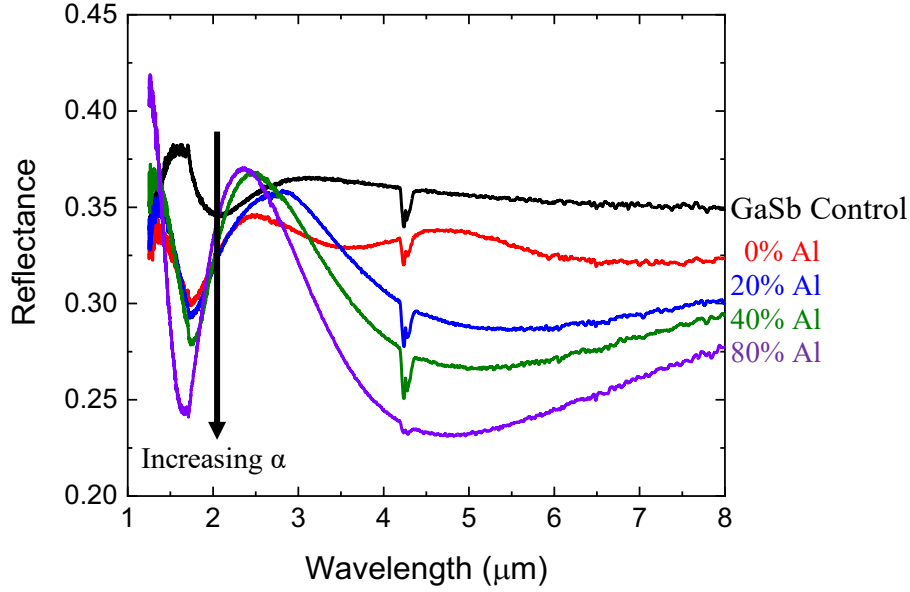
Figure 5. Optical spectra from AlInAsSb films lattice-matched to GaSb substrates. The aluminum composition of each is noted as a percentage of the group-III mole faction.

| (a) | (b) | (c) |
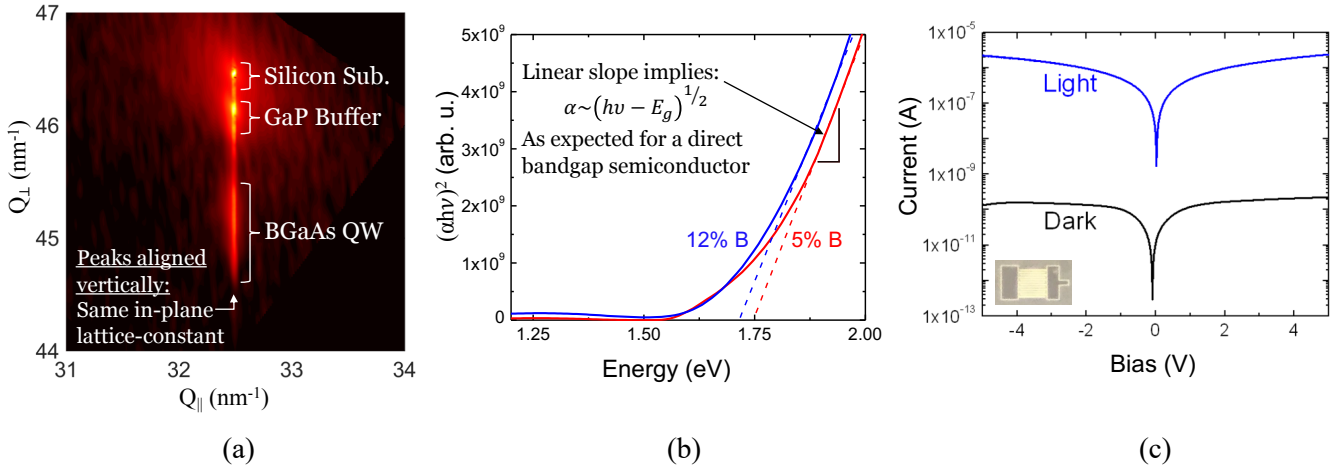
Figure 6. Illustrative results on BGaAs grown on GaP-on-Si and GaP substrates. (a) X-ray diffraction (XRD) reciprocal space map showing a BGaAs/GaP quantum well is coherent to the GaP and Si underlayers (all peaks lie along a vertical line, indicating they all share the same in-plane lattice-constant). (b) Absorption measurements of BGaAs films on (transparent) GaP substrates, showing a direct-gap absorption edge, consistent with theoretical predictions. (c) Current-voltage characteristics of a prototype BGaAs/GaP metal-semiconductor-metal photodetectors under dark (black) and light (blue) conditions as a device proof-of-concept.

3.1.3. Direct Bandgap Materials Lattice-Matched to Silicon

The fundamental challenge with silicon as a photonics platform is the lack of a direct-bandgap, type-I quantum well, diode laser materials system that can be lattice-matched to silicon. Unfortunately, existing monolithic approaches (i.e. grown directly on Si) have not yielded direct-bandgap materials that can be lattice-matched, or nearly lattice-matched, to silicon. Introducing boron (B) into GaAs has enabled the first direct-bandgap semiconductor alloy system that can be lattice-matched to silicon. In particular, our recent breakthrough in the growth of high B% BGaAs alloys has yielded the first type-I

direct bandgap quantum well materials system that can be lattice-matched to silicon. Growth results on GaP and GaP-on-Si templates are summarized in **Figure 6**. As seen in the X-ray diffraction (XRD) reciprocal space map in **Figure 6a**, we have produced *coherent* BGaAs/GaP quantum wells with <1.5% strain on silicon. We have also demonstrated thicker coherent films ideal for photodetectors.

This DURIP has been instrumental in determining that these materials are direct bandgap, via transmission and reflection measurements. Specifically, using thicker films grown on (transparent) GaP substrates, we have determined the absorption spectrum of BGaAs shown **Figure 6b**. Using the Tauc plot approach – where the product of the absorption coefficient, α, and the photon energy, *hv*, is squared and plotted against *hv* – allows for (1) determination of the bandgap (zero crossings of dotted lines in **Figure 6b**), as well as (2) determining whether the material is direct bandgap (linear slope above the bandedge). Specifically, for a direct bandgap semiconductor, this quantity should increase linearly above the bandgap energy, E_g. Since $(\alpha hv)^2 = hv - E_g$ rises linearly with photon energy in **Figure 6b**, this is consistent with a direct-bandgap, both in spectral shape and in magnitude. We have also demonstrated proof-of-concept BGaAs MSM photodetectors on a transparent GaP substrate, shown in **Figure 6c**.

3.1.4. Dissimilar Materials Integration: Semiconductors, Metals, and Dielectrics

We have been studying the epitaxial integration of metals and dielectrics with optically active semiconductor materials in order to create embedded optical structures and devices. In pursuit of this goal, under an AFOSR MURI, we demonstrated wavelength-scale silicon dioxide gratings embedded in high-quality GaAs and InAs grown by MBE. The high refractive index contrast of these grating structures allows for a variety of unique features including unity reflection and guided mode resonance; indeed, the DURIP instrumentation has been instrumental in characterizing these optical properties.

From finite-difference time-domain (FDTD) calculations, this material system was projected to have significant changes in reflectivity associated with interference between the planar top surface of the GaAs/Air interface and the high-contrast gratings. To characterize reflectivity, FTIR spectroscopy was used to measure the reflectivity of sample structures in the window of transparency from 1.25-5 µm. As control, two structures were measured, the grating as-fabricated without regrowth and an unpatterned MBE-grown GaAs samples, as these were anticipated to have limited changes in reflectivity over this spectral range.

The measured reflectivity of all samples is shown in **Figure 7a**. As expected, changes in reflectivity were observed in the encapsulated grating sample (black curve) taking the form of oscillations associated with interference fringing. Also, as expected, constant reflectivity was observed in both controls at the level of the theoretical response near 30%. This confirms that the changes in reflectivity are a result of the interaction between the planar GaAs top surface and encapsulated high-contrast grating. As shown in **Figure 7b**, we found excellent agreement between the FDTD reflectivity (and transmittance) spectrum and the experimental FTIR spectra.
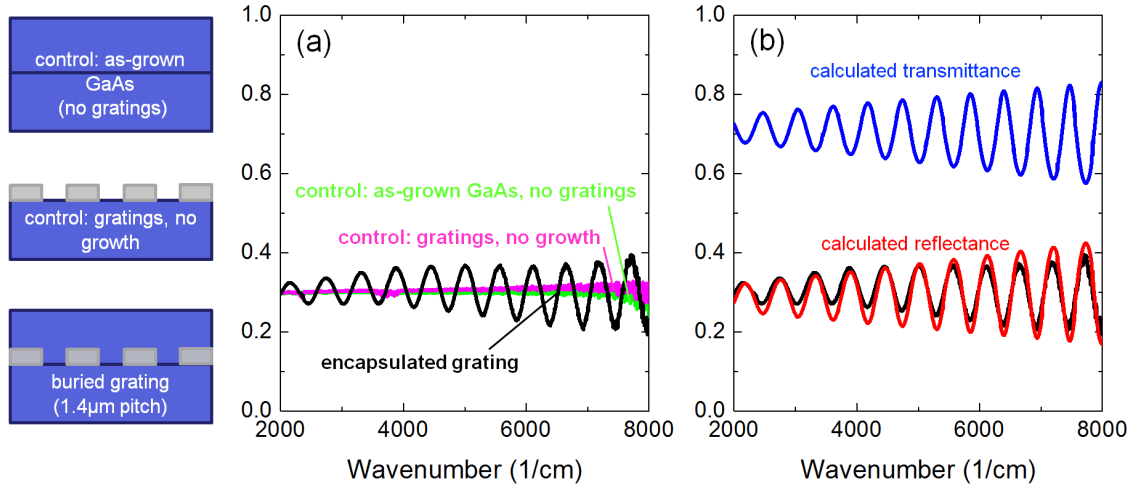
Figure 7. (a) Reflectivity spectra of encapsulated grating sample (black curve) and its two controls, as-grown GaAs with no grating (green curve) and as-fabricated grating without growth (magenta curve). Left: Sample structures. (b) FDTD reflectivity (and transmittance) spectrum closely matches the FTIR-measured grating spectra.

The FTIR was particularly essential when we investigated the post-growth selective lateral etching of the silicon dioxide gratings to increase the achievable refractive index contrast in these structures. The lateral etching process, illustrated in **Figure 8a**, was monitored by observing the intensity of the silicon dioxide resonance in the FTIR reflectance spectrum, seen in **Figure 8b**. The absence of the absorption peak at 1063 cm^{-1} indicates complete removal of the silicon dioxide. This demonstrates a process for the formation of epitaxially embedded air nanostructures with high refractive index contrast for applications in enhanced nanophotonic devices.

(a)   (b)
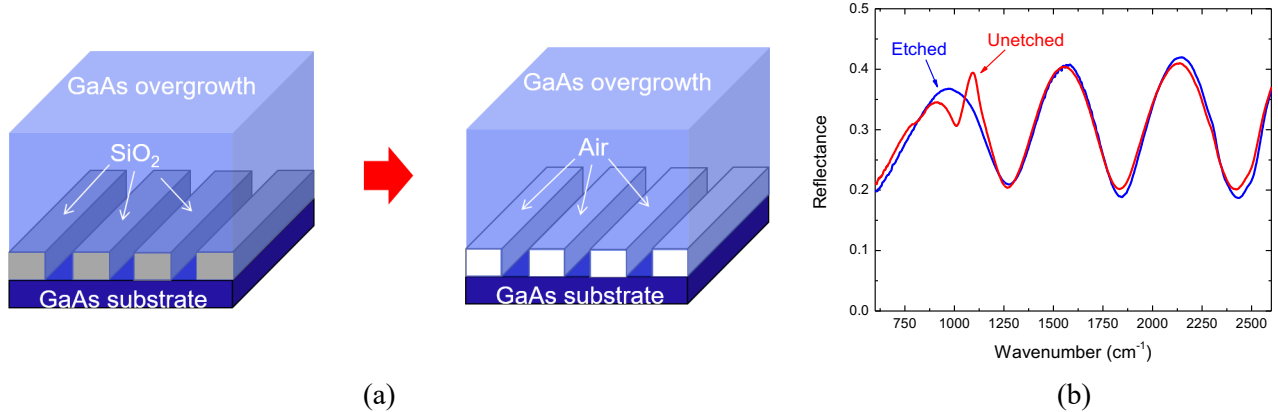
Figure 8. (a) Post-growth etching of the silica features to increase dielectric contrast. (b) The disappearance of the silica absorption resonance at 1063 cm^{-1} was used to determine complete removal of the silicon dioxide.

Through an AFOSR program, we also investigated whether it was similarly possible to embed patterned semimetal layers into III-V matrices, using a combination of *ex situ* patterning and *in situ* selective-area growth. To this end, we developed a patterning/regrowth process and characterized the deposition of semimetallic ErAs on a variety of V-groove templated surfaces using a variety of electrical, optical, structural, and chemically-sensitive techniques.

8

To study the optical properties of ErAs deposited on templated substrates, spatially-resolved reflectivity spectra were collected with the 36x objective of the Bruker Hyperion 1000 IR microscope and spectrally-resolved with the Bruker Vertex 80V FTIR. Line scan reflectivity spectra, normalized to the reflectivity of a gold standard, are plotted in **Figure 9**. These are 75 line scans taken 1.023 μm apart. We attribute the abrupt rise in reflectivity beyond ~15 μm to the plasma frequency of the n-type GaAs substrate. At shorter wavelengths, there are a variety of spectral features that are significantly more pronounced in the samples with ErAs (**Figure 9b** and **9c**) than the control without ErAs (**Figure 9a**). While this is very encouraging, though we do not yet know if these are truly due to wire formation or simply increasing the surface reflectivity, due to the large magnitude of the ErAs dielectric constant at these wavelengths, which will be addressed most directly with chemically-sensitive techniques like energy-dispersive X-ray spectroscopy (EDS) or X-ray photoelectron spectroscopy (XPS).

| (a) | (b) | (c) | (d) |
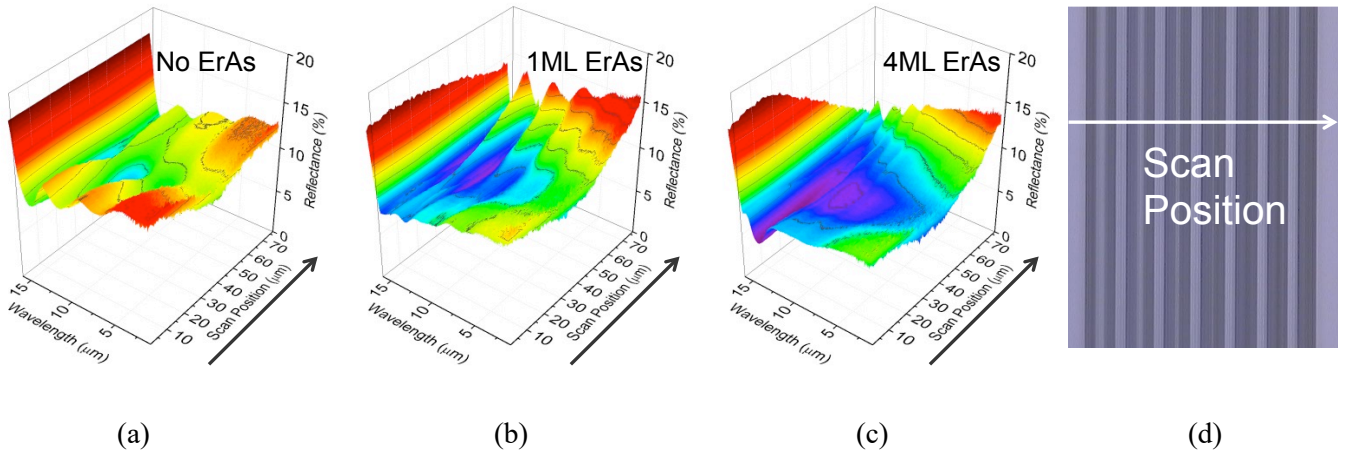
Figure 9. Optical reflectivity of V-groove structures, as a function of wavelength and position, measured with a FTIR and IR-microscope. (a) Patterned ErAs-free control, (b) 1 ML equivalent ErAs deposition, (c) 4 ML equivalent ErAs deposition, and (d) plan-view microscope image showing the measurement direction. Arrows indicate the scan direction.

3.2. Collaborations

The FTIR system has been instrumental in allowing us to measure microscopic material and geometric features that are readily identifiable in the near to mid-IR. In collaboration with Prof. Mikhail Belkin's group at UT, as shown in **Figure 10**, we were able to use our FTIR to measure the polarization-dependent response of nonlinear intersubband polaritonic metasurfaces. These devices allow desirable nonlinear device performance, such as frequency mixing, to occur at significantly lower pumping intensities that are below materials' damage threshold. This measurement would not have been possible without the FTIR and Hyperion microscope because these micron-scale features are very sensitive to orientation due to their strong polarization dependence. With the FTIR and microscope, we could isolate individual metasurfaces and insure they were correctly aligned – neither would be possible with a traditional FTIR nor optical reflectance set-up.
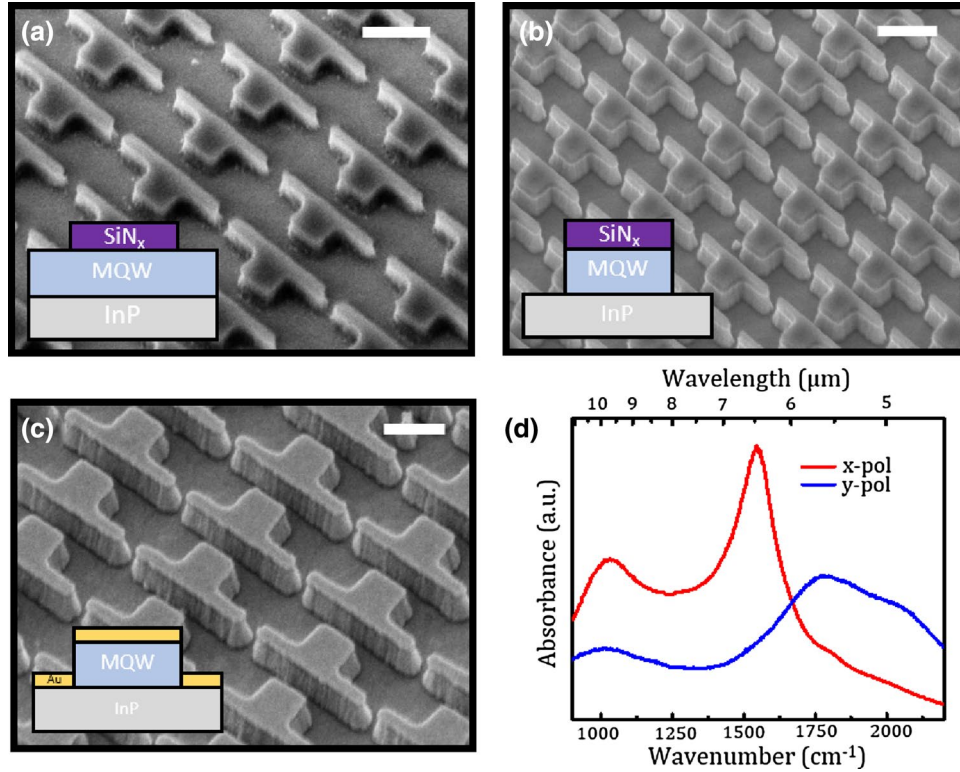
Figure 10. (a)–(c) Perspective scanning electron microscope images (rotated in-plane by 45° and tilted 30° from normal) of the intermediate steps in fabrication of an incomplete-metal-back-plane metasurface. The inset graphic depicts a side view of the material stack present in each step. (a) Image of the SiN_x dielectric hard mask used to etch the multi-quantum wells (MQW) following an electron-beam lithography step. (b) Image of the MQW nanoresonators capped with SiN_x following an inductively coupled plasma etch. (c) Image of the fabricated metasurface following removal of the SiN_x hard mask and gold evaporation formation of the incomplete metal backplane and plasmonic-cap. (d) Linear absorption spectra for x- and y-polarized light (red and blue curves, respectively) of the fabricated incomplete- backplane metasurface

We used the same capabilities to characterize the properties of optically active structures fabricated by "point-and-shoot" strategies by our collaborator Prof. Yuebing Zheng at UT. Prof. Zheng's group fabricated and modeled the structures and we used the Bruker Vertex v80 FTIR and IR microscope to confirm their simulations. As shown in **Figure 11**, site-specific fabrication of optically active Ag rings were demonstrated by inducing stable microbubbles over an Au nanoisland substrate, generated using a continuous-wave laser at low power (≈0.5 mW μm^{-2}), with representative reflectance spectra shown in **Figure 12**.

$$\frac{}{8\varepsilon_0 c}\left|\quad\right|^2 \quad ,$$

10
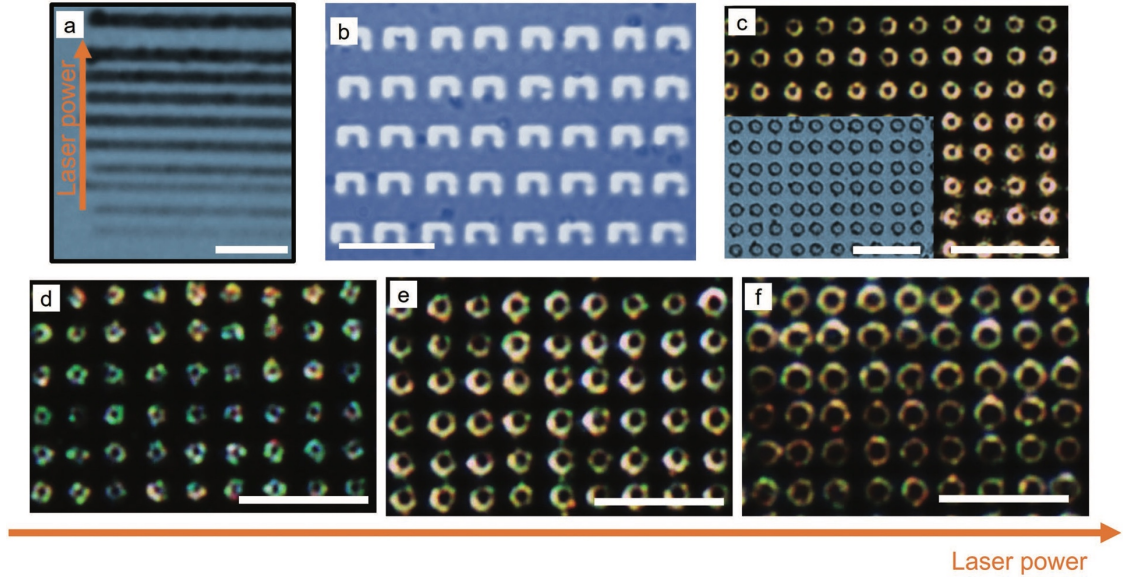
Figure 12. (a) Fabrication of Ag lines by a laser beam below the bubble-generation threshold power. The linewidth increases when the laser power is increased from 0.2 to 0.5 mW μm^{-2}. The bubble is observable when the laser beam is at the end of the line. (b) Arrays of Ag inverted-U structures fabricated by a laser beam below the bubble-generation threshold power. (c) Dark-field optical image of an Ag ring array fabricated at a laser power of 0.75 mW μm^{-2}. The inset shows the bright-field optical image. (d)–(f) Dark-field optical images of arrays of Ag rings of variable sizes. The incident laser power is (d) 0.55, (e) 0.81, and (f) 0.95 mW/μm^2. The scale bar is 10 μm for all the panels.
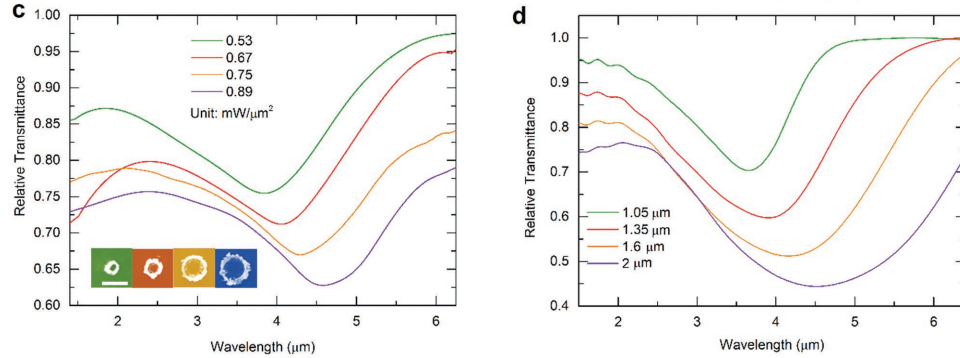

Figure 13. (a) The relative transmittance spectra of the arrays of Ag rings fabricated at the variable laser power. The spectra were normalized with respect to that of the Au nanoisland substrate as background. The inset shows representative SEM images of four individual rings that increase their diameters (1.08, 1.35, 1.67, and 2.02 μm) when the incident laser power changes from 0.53 to 0.89 mW μm^{-2}.

With Prof. Zheng's group, we also studied the optical properties of graphene metasurfaces with moiré patterns, fabricated via a cost-effective and scalable technique: moiré nanosphere lithography. The experimental measurements shown in **Figure 14** that the graphene moiré metasurfaces support tunable and multiband optical responses, due the size and shape dependences of surface plasmon resonance modes of graphene nanostructures.
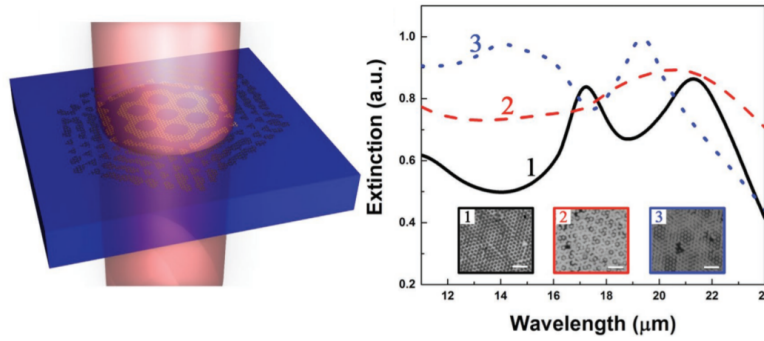
Figure 14. (Left) Schematic illustration of transmission extinction measurement of graphene moiré metasurfaces. The graphene nanostructures illuminated by incident light are excited to support surface plasmon resonances, resulting extinction in transmission. (Right) Measured extinction spectra of three graphene moiré metasurfaces with different patterns. The black and white areas in SEM images are graphene and substrates, respectively. The scale bars are 1.5 μm.

Black phosphorus (BP) has attracted rapidly growing attention for high speed and low power nanoelectronics owing to its compelling combination of tunable bandgap (0.3 to 2 eV) and high carrier mobility (up to ∼1000 cm^2/V-s) at room temperature. With Deji Akinwande's group at UT, we reported the first radio frequency (RF) flexible top-gated BP thin-film transistors on highly bendable polyimide substrate for GHz nanoelectronics applications. <u>The FTIR was instrumental in enabling us to determine the fundamental bandgap of the mechanically exfoliated black phosphorus flakes that functioned as the semiconducting channels.</u> The BP flake thicknesses were only 10−25 nm thick, which made for a challenging absorption experiment; additionally the flakes were only a few microns in lateral extent, as seen in the representative optical microscopy image **Figure 15a**. Therefore, the scanning IR microscope functionality was essential for the absorption measurements.
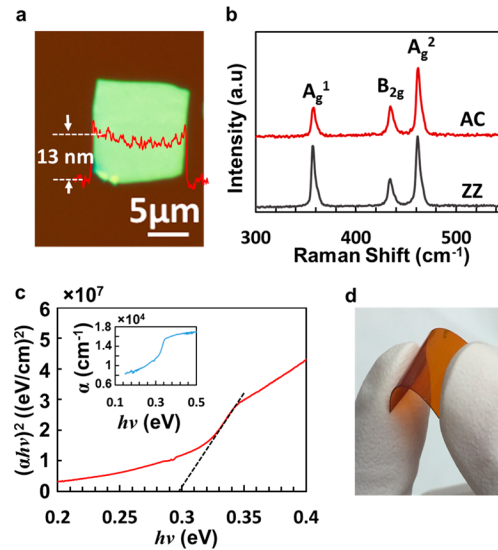
Figure 15. (a) Optical image of multilayer BP flake with uniform thickness of 13 nm as determined by AFM shown as the red line. (b) Raman spectrum of a typical BP flake with incident laser polarization within a close affinity to AC and ZZ directions, respectively. A 532 nm green laser was used to obtain the Raman spectrum. (c) A representative Tauc plot for estimating the optical bandgap, which confirms a gap of ∼0.3 eV in the bulk limit. Insert is the absorption coefficient of BP derived from Fourier transform infrared (FTIR) spectrum. (d) Picture of fabricated flexible TG BP devices on highly bendable polyamide substrate.

The flake in **Figure 15a** had uniform thickness of ~13 nm verified by atomic force microscopy (AFM). The crystalline nature of BP was verified by Raman spectroscopy with incident laser (λ = 532 nm) polarized along both armchair (AC) and zigzag (ZZ) directions, as shown in **Figure 15b**, where the ratio among characteristic peaks of A_g^1, B_{2g}, and A_g^2 clearly indicates the in-plane orientations. For B_{2g}, and Ag exfoliated BP flakes with thickness more than 10 nm, the theoretical bandgap is ~0.3 eV, which is confirmed in **Figure 15c** by Fourier transform infrared (FTIR) spectroscopy that is represented as a Tauc plot ($(\alpha h\nu)^2 = h\nu - Eg$) an established method for determining the optical band gap. $h\nu$ is the photon energy, Eg is the optical bandgap, and α is the absorption coefficient. As shown in **Figure 15d**, highly bendable Kapton polyimide (PI) sheets ~125 μm thick were adopted as the substrate for the flexible BP transistors with double sided solution-based PI thin film coating and curing process applied to smoothen the substrate to about 1 nm surface roughness.

4. References

[1] V. M. Glazov, R. A. Akopyan, and E. I. Shvedkov, "Investigation of the relationship between the electron density and solubilities of sulfur, selenium, and tellurium in indium arsenide," *Sov. Phys. Semicond.*, vol. 10, no. 4, pp. 378–380, Apr. 1976.